

GT2011-45* - *

COMBUSTION OF NATURAL GAS, HYDROGEN AND BIO-FUELS AT ULTRA-WET CONDITIONS

Sebastian Göke*, Steffen Terhaar, Sebastian Schimek, Katharina Göckeler, Christian O. Paschereit
Chair of Fluid Dynamics
- Hermann-Föttinger-Institute -
Technische Universität Berlin
Germany

ABSTRACT

Humidified Gas Turbines promise a significant increase in efficiency compared to the dry gas turbine cycle. In single cycle applications, efficiencies up to 60% seem possible with humidified turbines. Additionally, the steam effectively inhibits the formation of NO_x emissions and also allows for operating the gas turbine on hydrogen-rich fuels.

The current study is conducted within the European Advanced Grant Research Project GREENEST. The premixed combustion at ultra wet conditions is investigated for natural gas, hydrogen, and mixtures of both fuels, covering lower heating values between 27 MJ/kg and 120 MJ/kg. In addition to the experiments, the combustion process is also examined numerically.

The flow field and the fuel-air mixing of the burner were investigated in a water tunnel using Particle Image Velocimetry and Laser Induced Fluorescence. Gas-fired tests were conducted at atmospheric pressure, inlet temperatures between 200°C and 370°C, and degrees of humidity from 0% to 50%.

Steam efficiently inhibits the formation of NO_x emissions. For all tested fuels, both NO_x and CO emissions of below 10 ppm were measured up to near-stoichiometric gas composition at wet conditions. Operation on pure hydrogen is possible up to very high degrees of humidity, but even a relatively low steam content prevents flame flashback. Increasing hydrogen content leads to a more compact flame, which is anchored closer to the burner outlet, while increasing steam content moves the flame downstream and increases the flame volume.

In addition to the experiments, the combustion process was modeled using a reactor network. The predicted NO_x and CO emission levels agree well with the experimental results over a wide range of temperatures, steam content, and fuel composition.

NOMENCLATURE

ϕ	Equivalence ratio (-)
Ω	Degree of humidity (-)
σ	Variance of concentration fluctuations (-)
τ	Mean Residence time (s)
τ'	Decay constant of the concentration response (s)
c	Fuel concentration (-)
\bar{c}	Mean fuel concentration (-)
D_H	Hydraulic diameter (mm)
J	Momentum ratio (-)
k_{rec}	Recirculation rate (-)
\dot{m}_{tot}	Total mass flow rate (air plus steam) (kg/s)
S	Swirl number (-)
T_{ad}	Adiabatic flame temperature (°C)
u	Velocity (m/s)
$U_{s/t}$	Spatial / temporal degree of unmixedness (-)
\dot{V}	Volume flow rate (m ³ /s)
x	Axial coordinate (m)

*Address all correspondence to this author, sebastian.goeke@tu-berlin.de.

INTRODUCTION

Gas turbines are vital for the generation of electricity in power plants, since they have a high efficiency, emit low emissions, and are capable of quickly responding to changes in electricity demand. Currently operating mostly on natural gas or fuel oil, gas turbines of the next generation must also be able to burn a variety of additional fuels such as hydrogen, syngas from coal gasification, or bio-fuels of variable composition.

In order to further increase efficiency of current gas turbine technology, however, operating pressure and turbine inlet temperature must be raised. This leads to complex technological problems, for example, for the cooling system or for the lifetime of the hot parts. Additionally, NO_x emissions will be significantly increased at higher combustion temperatures.

In humid gas turbines (HGT), water or steam injection is used to increase efficiency without having to increase the turbine inlet temperature. In addition to the higher efficiency, the power is augmented, NO_x emissions are reduced, and the steam can be efficiently used for cooling of the combustion chamber liner and the turbine blades. Humid gas turbines thus seem to be capable of achieving similar or even higher efficiencies compared to combined cycle power plants, at significantly reduced cost and plant complexity, as no steam turbine is required [1,2].

A variety of different HGT cycles have been developed. Among them are the steam injected gas turbine cycle (STIG), which includes the Cheng cycle, and the evaporative gas turbine cycle (EvGT) [3–8]. While the injection of small amounts of steam for NO_x control has been employed in commercial gas turbines for several years already, a pilot plant based on the EvGT cycle has been built in Sweden [9]. More recently, a 4 MW pilot plant using a humidification tower has been built by Hitachi with promising initial results [10,11].

So far, humid gas turbines have usually been investigated with steam levels not higher than 15% to 20%. In the current study, the combustion process is investigated for significantly higher steam contents of up to 50%, operating at near-stoichiometric conditions with low NO_x and CO emissions. This promises a further increase in efficiency and also allows for post-combustion CO_2 capture at low cost, since the concentration of CO_2 reaches the highest possible value for air breathing gas turbines after condensation of the steam.

Concerning syngas or hydrogen fuel, current gas turbine technology is not able to operate on these fuels efficiently and at low emissions. This is mostly caused by the high reactivity of hydrogen, which leads to a flame speed that is about one order of magnitude higher than that of natural gas, resulting in an increased risk of flame flashback [12–14]. The presence of hydrogen in the fuel also leads to increased NO_x emissions [15,16]. Several research programs currently pursue the development of gas turbines to operate on (high-) hydrogen fuel [17–20]; one approach is to dilute the fuel with small quantities of steam; however, this usually results in reduced efficiencies in dry gas turbine

cycles. In humid gas turbines, however, steam is readily available and allows for the operation on hydrogen-rich fuels and hydrogen at low NO_x emissions and high plant efficiency.

A number of studies have investigated the influence of steam on the combustion process for natural gas as well as for syngas and hydrogen. Most publications are limited to relatively low degrees of humidity, and to non-premixed flames. It was shown for a wide variety of fuels that diluting the fuel with steam significantly reduces the laminar burning velocities [12,21].

Concerning NO_x emissions, steam injection affects the emission formation in two ways [22–26]. It reduces the flame temperature, and therewith, restrains the thermal NO_x formation pathway which contributes most to overall NO_x emissions at temperatures above approximately 1800 K. The steam also directly affects the reaction kinetics by changing the concentration of active species which are involved in the NO_x formation. Thus, even at the same flame temperature, NO_x emissions are significantly reduced. The influence of steam injection on CO emissions depends strongly on the combustor configuration. While some authors state that steam injection can increase CO emissions [27], others found that CO is not affected by humidity [28], or even slightly reduced [29].

In the current study, the premixed combustion of hydrogen, natural gas, and mixtures of both gases is investigated over a wide range of equivalence ratios from lean blowout to near-stoichiometric conditions and steam content in the air between 0% and 50%. Fuels with lower heating values between 2.7 MJ/kg and 120 MJ/kg are assessed in this study.

Insight into the the flow field and the fuel-air mixing process of the employed generic combustor was gained by conducting experiments in a water tunnel. The results also serve as a basis for the modeling of the combustion process.

The influence of steam content and fuel composition on emission formation, flame stability, and flame shape was investigated in gas-fired tests.

Based on the results of both the water tunnel experiments and the gas-fired tests, a reactor network was designed to model the combustion process and gain further insight into the emission formation at ultra-wet conditions.

EXPERIMENTAL SETUP

Combustion Test Rig

Preheated air and overheated steam are mixed upstream of the burner. The experiments are conducted with a generic, premixed burner. For the current study, a constant swirl number of $S = 0.7$ is used. Detailed information about the combustor setup is given in [30]. The cylindrical combustion chamber is made of quartz glass and has a length of 300 mm, followed by a water-cooled exhaust tube of 1 m. The diameter is 200 mm. The test rig is operated at atmospheric conditions.

Temperatures were measured at different axial locations downstream of the burner outlet. The combustor inlet temperature was measured in the mixing tube of the burner, downstream of the fuel injection. It is controlled in order to have a deviation of the set value of less than ± 5 K.

For typical measurements, the test rig is operated at a constant mass flow rate of air and steam, while the amount of fuel is reduced in steps of $\Delta\phi = 0.05$ from stoichiometric conditions to lean blowout.

Exhaust gas is extracted from the combustor 850 mm downstream of the burner outlet, and transported through a heated tube to a cold steam trap to remove humidity. It is then analyzed for CO, NO, NO₂, O₂ and CO₂ on a dry basis.

An intensified CCD camera with a bandpass filter at 308 nm is used to give the spatial distribution of OH* chemiluminescence, which correlates with the intensity of the chemical reaction and is used to determine the flame position.

Degree of humidity. Throughout the study, the steam content is described by the degree of humidity

$$\Omega = \frac{\dot{m}_{steam}}{\dot{m}_{air}}, \quad (1)$$

where \dot{m}_{steam} is the mass flow rate of steam, and \dot{m}_{air} the mass flow rate of air. The total mass flow rate is $\dot{m}_{tot} = \dot{m}_{air} + \dot{m}_{steam}$.

Operating conditions. The gas-fired experiments were conducted with combustor inlet temperatures of 200°C and 370°C, a total mass flow rate of $\dot{m} = 180$ kg/h = 0.05 kg/s, and degrees of humidity between $\Omega = 0\%$ and $\Omega = 50\%$. The range of evaluated fuels and their respective lower heating values are given in Table 1. The concentration of methane in the natural gas is above 98%. The flow rates of the water tunnel experiments were scaled to match the operating conditions of the gas-fired tests.

Water Test Rig

The cold flow experiments were carried out in a vertically-oriented water tunnel. The test section has a square cross-section, consisting of four glass windows, providing full optical access to the mounted combustor model.

Additionally, a volume flow of water could be injected through the premix-holes into the mixing tube, in order to simulate fuel injection. Several studies [31] have shown that the mixing of jets in a cross flow mainly depends on the momentum ratio J of the jet to the main flow. Since the momentum ratio is also the governing parameter for the influence on the flow field, the injected volume flow could be adjusted for simulating different

TABLE 1: COMPOSITION AND LOWER HEATING VALUE OF ASSESSED FUELS

Fuel composition <i>%mass</i>	Fuel composition <i>%vol</i>	LHV <i>MJ/kg</i>	LHV <i>MJ/m³</i>
100% NG	100% NG	50	33
90% NG, 10%H ₂	53% NG, 47%H ₂	57	22
80% NG, 20%H ₂	33% NG, 67%H ₂	64	18
30% NG, 60%N ₂ , 10%H ₂	21% NG, 24%N ₂ , 55%H ₂	27	12
50%H ₂ , 50%N ₂	93%H ₂ , 7%N ₂	59	9
100%H ₂	100%H ₂	120	10

fuel compositions, densities, and fuel to air equivalence ratios.

$$J = \frac{u_{fuel}^2 \cdot \rho_{fuel}}{u_{air}^2 \cdot \rho_{air}} \quad (2)$$

Flow velocities were measured using Particle Image Velocimetry (PIV). The laser sheet was generated using a Continuum Nd:YAG pulse laser (20mJ per pulse) and 400 picture pairs (1024x1024px²) per measurement were recorded by a CCD camera at a frequency of 4 Hz. The images were processed with a final interrogation size of 16x16 px² with 50% overlap, resulting in a resolution of 1.3 mm. The data was filtered for outliers and interpolated from adjacent interrogation areas.

The mixing quality of the injected volume flow through the premix holes with the main flow was assessed at the burner outlet using Laser Induced Fluorescence (LIF). A cw-laser (5W Nd:YAG) generated an intense light sheet 2 mm downstream of the burner outlet. A high-speed CCD camera recorded the mixing of the steadily injected fluorescent dye (Rhodamine G6) with a frame rate of 60 Hz. The concentration of the 1180 recorded pictures (640x576 px²) were calculated using a reference picture of known dye concentration.

A vertical light sheet was used to measure the unsteady mixing behavior where a high concentration of dye is injected into the steadily injected water flow as a short pulse (150 ms) simulating a Dirac delta pulse.

The investigated configurations included fuel to air momentum ratios from $J = 0$ to $J = 13$ at a water mass flow rate of 6.8 m³/h (1.89·10⁻⁴ m³/s), which is equivalent to air mass flow rates of 180 kg/h ($T_{air} = 573$ K, $\Omega = 30\%$), and a Reynolds number of 26,500 based on the hydraulic diameter of the burner outlet. The swirl number was set to a value of $S = 0.7$, assuring vortex breakdown under all measured configurations.

Table 2 gives an overview of momentum ratios used as well as corresponding fuel compositions and equivalence ratios.

TABLE 2: ASSESSED MOMENTUM RATIOS FOR THE NON-REACTING MEASUREMENTS

J	Fuel	ϕ
0	No Injection	0
1	Methane	0.6
3 - 6.7	Hydrogen	0.7 - 1
13	50% Hydrogen + 50% Nitrogen	0.5

Reactor Network

A reactor network was designed to model the combustion process. The simulations were conducted with the software *Cantera* [32]. Two different reaction mechanisms were used: the GRI-Mech 3.0 mechanism [33] and the “Detailed reaction mechanism for small hydrocarbons combustion, Release 0.5” by Konnov [34]. The network consists of several perfectly stirred reactors (PSR) for the main flame zone followed by a plug-flow reactor (PFR) for the post-flame zone (Fig. 1). Since plug-flow reactors are not available in *Cantera*, a series of 20 perfectly stirred reactors was used instead for the post-flame zone, which approximates the PFR with sufficient accuracy.

The design of the reactor network is based on the experimental results of both the water tunnel and the gas-fired tests, and is explained in detail later in this publication.

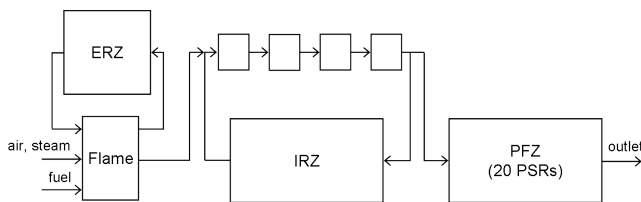


FIGURE 1: LAYOUT OF REACTOR NETWORK

RESULTS OF FLOW FIELD INVESTIGATIONS

The combustor aerodynamics at non-reacting conditions are investigated in a water tunnel facility. Though combustion has an effect on the flow field, it can be assumed that the influence of

burner geometry is qualitatively similar for the non-reacting and reacting flow. In particular, fuel air mixing can be investigated accurately, since combustion has only a minimal effect on the upstream flow field.

Flow Field Description

The flow field downstream of the burner is typical for swirl-stabilized burners. As shown in Fig. 2, three regions can be identified¹: an annular jet emanating from the mixing tube with a velocity of 65 m/s, an internal recirculation zone (IRZ) generated by vortex breakdown and an external recirculation zone (ERZ) induced by the area change. In between the regions, turbulent shear layers are produced, providing a continuous exchange of species between the regions.

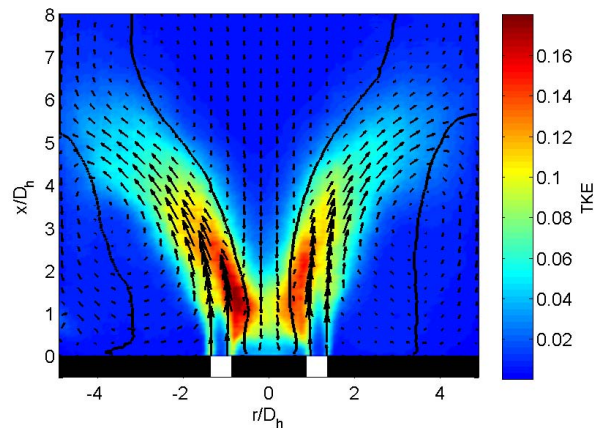


FIGURE 2: FLOW FIELD, $u = 0 \text{ m/s}$ LINE AND TURBULENT KINETIC ENERGY, ONLY EVERY 6TH VECTOR IS SHOWN ($J=0$)

The flame position is typically found in the inner or outer shear layer where flow velocities are low and equal to the turbulent flame speed. However, the actual position of the flame also depends on other parameters such as fuel composition, flame speed, and the effect of heat release on the flow field, and cannot be directly determined only from the cold flow.

The momentum of the injected fuel is substantially higher for fuels with a low LHV per volume, such as hydrogen or syngas, than for conventional fuels like methane. While the ratio of the injected volume to the main flow volume varies from less than 2.5% of the primary volume flow for lean methane combustion to more than 16% for nitrogen diluted hydrogen, the injected momentum varies from 2% to 30%. Since the swirl number is defined as the ratio of the axial flux of angular momentum to the

¹A comparably small centerbody wake can be identified as well when plotting the vectors at a higher resolution

axial flux of axial momentum, fuel injection in the axial direction has a decreasing effect on the swirl intensity.

This decrease could be observed in the measured swirl number, which decreases linearly with the injected fuel momentum. However, the swirl intensity remains strong enough to ensure stable vortex breakdown.

For a confined jet, the rate of entrainment at a specific axial position is equivalent to the recirculation rate, which is defined as the ratio of the recirculating volume flow \dot{V}_{rec} to the total volume flow \dot{V}_{tot} ,

$$k_{rec}(x) = \frac{\dot{V}_{rec}(x)}{\dot{V}_{tot}}. \quad (3)$$

The recirculation of hot reacting products is important for flame stabilization. Fig. 3 shows the recirculation rate of the IRZ for the various injection momentum ratios. As a result of the reduced swirl, it can be observed that primarily from $x/D=1$ to $x/D=3$, the recirculation rate is lower for high momentum ratios. The recirculation rate of the ERZ reaches up to 110%; however, from measurements of the reacting flow field for a similar combustor configuration, it is known that the recirculation rate of the ERZ is significantly lower at reacting conditions. Recirculation through the IRZ at reacting conditions is only marginally different, compared to that of the non-reacting flow field. In the current study, the recirculation rate measurements are used primarily for the design of the reactor network. The influence of recirculation on flame stability and emission formation at wet conditions was recently investigated by Gökeler et al. [30].

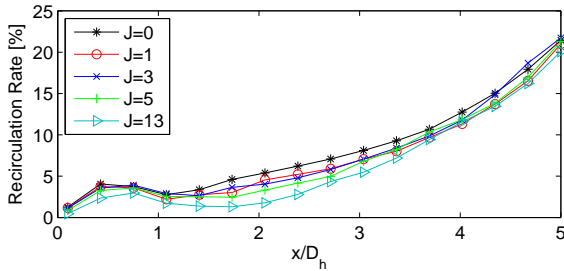


FIGURE 3: RECIRCULATION RATE OF THE INNER RECIRCULATION ZONE FOR THE NON-REACTING FLOW

Steady Mixing

Fuel-air mixing was assessed using the LIF technique. The injected volume flow was set in order to obtain similar momentum ratios as in the gas fired tests for H_2 and H_2+N_2 combustion

(Table 2). The mixing quality can be described by the degree of unmixedness, which is defined as

$$U_{s/t} = \frac{\sigma_{s/t}^2}{\bar{c}(1-\bar{c})}, \quad (4)$$

where \bar{c} is the mean fuel concentration, and $\sigma_{s/t}^2$, the spatial or temporal variance of the concentration fluctuations.

At wet conditions, the influence of fuel-air mixing on NO_x emissions is relatively low. However, a low degree of mixing also implies fuel-lean regions, which at wet conditions could lead to local quenching and therewith to high CO emissions and a reduced flame stability.

Measurements showed that for all investigated momentum ratios ($J=1$ to 13), the spatial degree of unmixedness U_s is below $2.5 \cdot 10^{-4}$ and the temporal degree of unmixedness U_t is below $4 \cdot 10^{-4}$. Thus, the fuel-air mixture can be regarded as almost homogeneous over the entire range of fuels.

Unsteady Mixing, Residence Time

Cold flow investigations provide valuable information about the parameters influencing residence time and the identification of zones of similar residence times that can be used for modeling the combustor using a reactor network. While a steady volume flow of undyed water was injected through the premix holes, a short pulse (150ms) of low volume flow, but very high dye concentration, was added to the injected water flow. In the flow field a zone near the burner outlet immediately shows a high but rapidly decreasing dye concentration. Afterwards the dyed fluid is transported through the turbulent shear layers into the ERZ and by a bypass-like zone near the walls into the IRZ.

By fitting an exponential function to the decay of the normalized concentration response (Fig. 4), the decay constant τ' of the response can be directly determined:

$$c_{fit}^*(t) = c_0 \cdot e^{-\frac{t-t_0}{\tau'}}, \quad (5)$$

where t_0 and c_0 represent the time and concentration at the beginning of the decaying response.

If the IRZ and ERZ act as perfectly stirred reactors and the input into the zone has the form of a Dirac pulse, the decay constant of the concentration response τ' is equivalent to the mean residence time τ of the zone. Therefore, a first-order approximation of the residence time can be derived from the decay constant.

$$\tau = \int_0^{\infty} e^{-\frac{t}{\tau'}} dt = \tau' \quad (6)$$

A spatial discretization of the flow field into 40×90 rectangles and subsequent calculation of the local decay constants

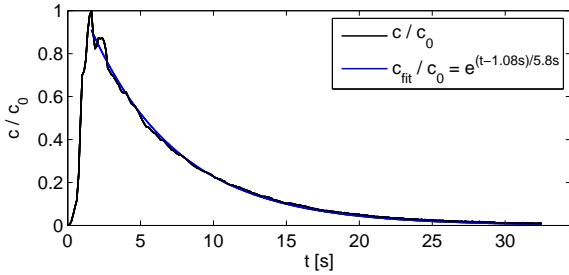


FIGURE 4: EXAMPLE OF A NORMALIZED CONCENTRATION CURVE AND THE FITTED EXPONENTIAL FUNCTION.

yields the spatial distribution of the decay constant in the combustion chamber as shown in Fig. 5. The aforementioned zones of the flow field, the annular jet with low decay constants ($\tau' < 1$ s), and the internal and the external recirculation zones with similar decay constants of $\tau' > 5$ s can be easily identified.

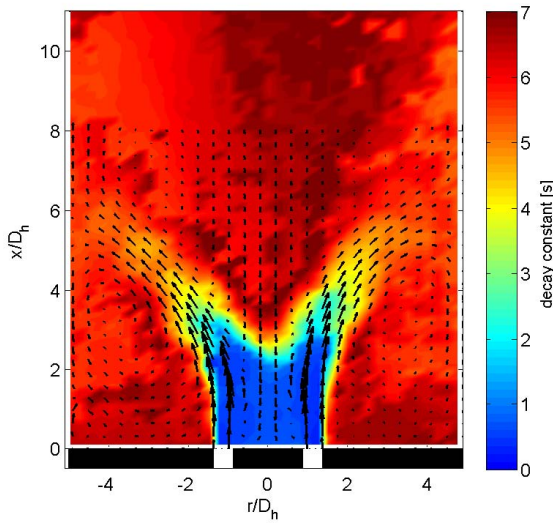


FIGURE 5: SPATIAL DISTRIBUTION OF THE DECAY CONSTANT. ($J=5$)

When trying to derive residence times from the decay constant, the simple relationship shown in Eq. 6 cannot be directly applied, because due to the exchange processes between the zones, the assumption of a Dirac pulse input into the recirculation zones is no longer valid. As a result, dyed fluid still enters the zones after the first pulse of dye, leading to a considerably higher decay constant τ' and suggesting a higher mean residence time τ than is actually present.

Scaling of cold flow residence times to reacting air flow velocities can be done by using the relationship between the residence time, the reactor volume, and volume flow rate ($\tau = V/\dot{V}$). However, the effect of heat release on the flow field, which leads to a change in sizes of the IRZ and ERZ, must be taken into account.

RESULTS OF GAS-FIRED EXPERIMENTS

The OH^* chemiluminescence images for the cases with 100% natural gas and 100% hydrogen are presented in Fig. 6 for an increasing degree of humidity. During operation of the test rig at wet conditions, the surface of the quartz glass combustor deteriorates within a couple of hours, thus affecting the absorption of the flame radiation. A quantitative comparison of the intensity of the OH^* radiation between the presented images is, therefore, not possible. This also leads to the asymmetry in OH^* intensity in some of the presented images.

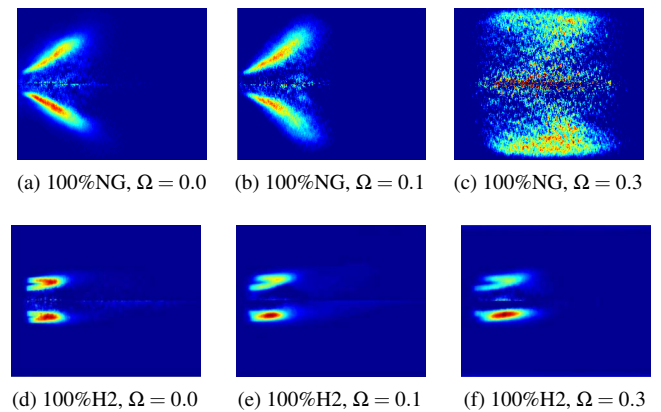


FIGURE 6: ABEL DECONVOLVED OH^* CHEMILUMINESCENCE IMAGES OF THE FLAME ($T_m = 370^\circ\text{C}$, $\phi = 0.8$, SHOWING APPROXIMATELY TWO THIRDS OF THE QUARTZ GLASS COMBUSTOR LENGTH. ABEL DECONVOLUTION LEADS TO ARTEFACTS IN THE CENTER OF THE IMAGES.)

At dry conditions, the natural gas flame is tilted towards the combustor wall. It is located between the inlet jet and the inner recirculation zone and exhibits a relatively long reaction zone. In comparison, the hydrogen flame is significantly shorter and also located in the shear layer between the inlet jet and the outer recirculation zone. The flame is significantly less tilted. For the other assessed fuels, a transition from the long flame with natural gas to the short hydrogen flame occurs with increasing H_2 content. Wicksall et al. [35] performed PIV measurements of the reacting flow field using a similar burner as for the current study and found similar results. They explain these effects by the higher

momentum of the hydrogen flame caused by the earlier heat release and by the higher reactivity of hydrogen, which enables the flame to sustain the higher strain.

At wet conditions, the flame speed is reduced and the reaction rates are slower, which leads to a wider reaction zone and moves the maximum of the OH* radiation further downstream. The effect of humidity is strongest for natural gas and decreases with hydrogen content in the fuel. At a degree of humidity of $\Omega = 30\%$, the natural gas flame is distributed over a wide range. A substantial further increase in humidity is only possible if the combustor inlet temperature is also increased. For the hydrogen flame, this effect occurs at significantly higher degrees of humidity.

The influence of fuel composition and steam content on the flame length is presented in Fig. 7. The flame length is calculated from the OH* chemiluminescence images as the axial length, wherein 80% of the OH* chemiluminescence intensity is contained. Diluting the fuel with nitrogen has no significant impact on the flame length. The same holds for the axial position of the maximum of the OH*-chemiluminescence intensity, the flame stability, and also the NO_x and CO emissions. However, diluting hydrogen-rich fuels with nitrogen allowed for higher equivalence ratios at dry conditions without the flame being stabilized in the boundary layers of the mixing tube of the burner.

Although the effect of humidity is significantly lower for the hydrogen flame, it was possible to burn this fuel up to near-stoichiometric conditions without flashback, even at the lowest assessed degree of humidity of $\Omega = 10\%$.

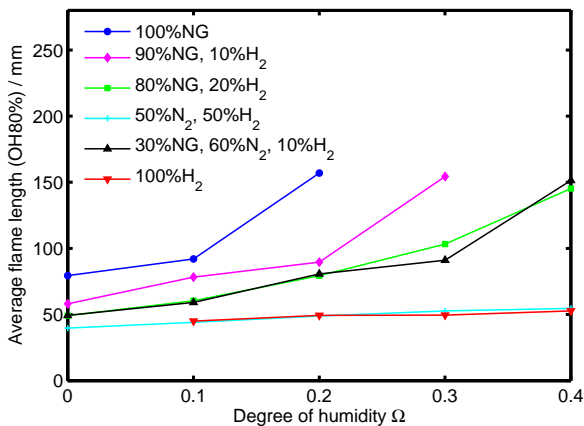


FIGURE 7: FLAME LENGTH - AXIAL DISTANCE WHEREIN 80% OF OH-CHEMILUMINESCENCE INTENSITY IS CONTAINED, AVERAGE FOR $\phi = 0.8 - 0.95$. ($T_{in} = 200^\circ\text{C}$)

Blowout Limit

Injecting steam both reduces the flame temperature and dilutes the oxidizer. Thus, with increasing steam content, higher equivalence ratios are required to prevent flame extinction. Figure 8 presents the blowout limits for the different fuels. The diagram shows the lowest required equivalence ratio for a stable flame; for equivalence ratios above the curves, the flame is stable, whereas the flame moves downstream and is finally blown out for operating points below the curves. For the tests with 100% H₂, flame blowout could not be achieved because the fuel mass flow was too low to be measured with the flow meter. In order to give an impression of the operating range with hydrogen, the lowest tested equivalence ratios are presented in Fig. 8.

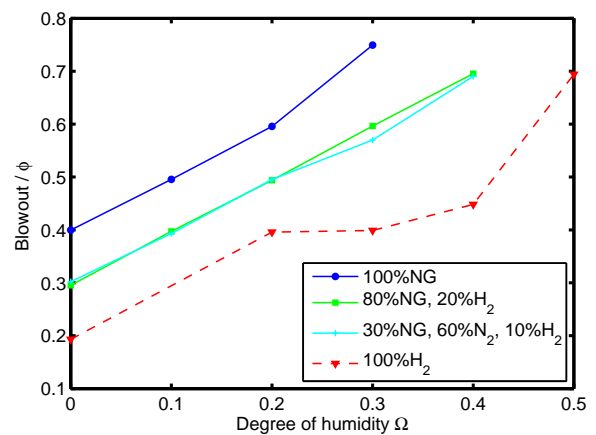


FIGURE 8: BLOWOUT LIMIT (FOR OPERATION ON HYDROGEN, THE LEANEST TESTED OPERATING POINTS ARE PRESENTED; THE ACTUAL FLAME BLOWOUT OCCURS AT LOWER EQUIVALENCE RATIOS. $T_{in} = 370^\circ\text{C}$)

With increasing hydrogen content in the fuel, the operational range is increased and the flame can sustain higher degrees of humidity. The maximum possible steam contents were not determined exactly in the experiments, but they are approximately $\Omega = 35\%$ for pure natural gas, and $\Omega = 45\%$ for the (80% NG, 20% H₂)-fuel mixture. Diluting the fuel with nitrogen has no effect on the blowout limit. Increasing the combustor inlet temperature improves the blowout limits for a given fuel, while reducing the inlet temperature leads to a narrower operational range. For $T_{in} = 200^\circ\text{C}$, the blowout curves are shifted towards higher equivalence ratios by approximately $\Delta\phi = 0.15$.

Emissions

The measured NO_x emissions for natural gas are presented in Fig. 9 together with the calculated adiabatic flame temperatures. At dry conditions, the emissions are relatively low for lean mixtures, but increase rapidly for temperatures above approximately 1700 K, above which the NO_x formation is dominated by the thermal pathway. At wet conditions, NO_x emissions are significantly reduced, even if the equivalence ratio is increased to achieve the same adiabatic flame temperature as at dry conditions. For operation on natural gas and degrees of humidity above $\Omega = 20\%$, NO_x emissions are below 10 ppm (at 15% O_2 , dry) up to stoichiometric conditions.

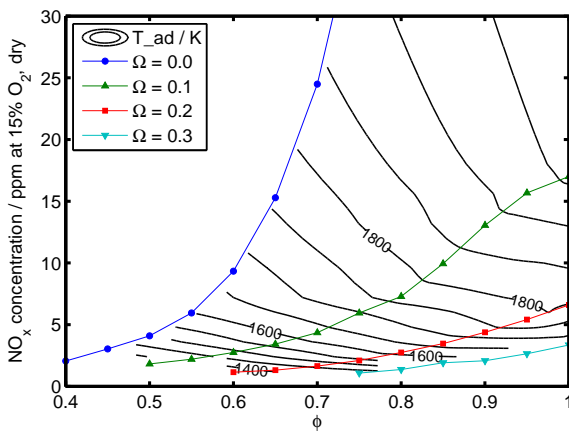


FIGURE 9: NO_x EMISSIONS FOR 100% NG

The NO_x concentration for the $\text{H}_2 + \text{NG}$ fuels based on the calculated adiabatic flame temperature is presented in Fig. 10. The actual flame temperature is estimated to be up to 150 K lower due to heat convection and gas radiation. For both dry and wet conditions, the methane-containing fuels lead to higher NO_x emissions than for pure hydrogen. This effect was also observed in other studies (e.g. [36]), where it is attributed to increased NO_x formation via the prompt pathway with increasing concentration of methane.

At wet conditions, the NO_x emissions of all assessed fuels are significantly lower. In addition to the reduction in flame temperature, humidity suppresses NO_x formation by affecting the reaction kinetics [23]. These effects lead to a significant decrease in overall NO_x production. Additionally, the increase in NO_x emissions with respect to flame temperature is substantially lower.

The CO emissions for the carbon-containing fuels are presented in Fig. 11, exhibiting the typical trend of practical com-

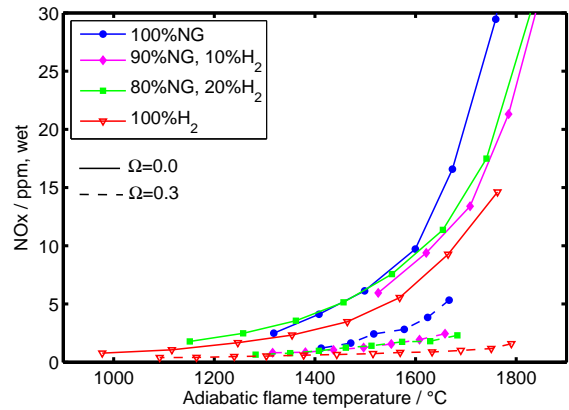
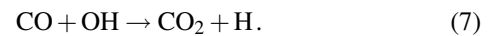


FIGURE 10: NO_x EMISSIONS FOR DIFFERENT FUELS

Combustion systems. The burnout of CO into CO_2 is dominated by one reaction:



If the residence time is long enough to reach equilibrium, CO emissions are mostly controlled by the concentrations of OH and CO_2 , and temperature. In the experimental setup for the current study, the combustor residence time is approximately 100 ms to 200 ms.

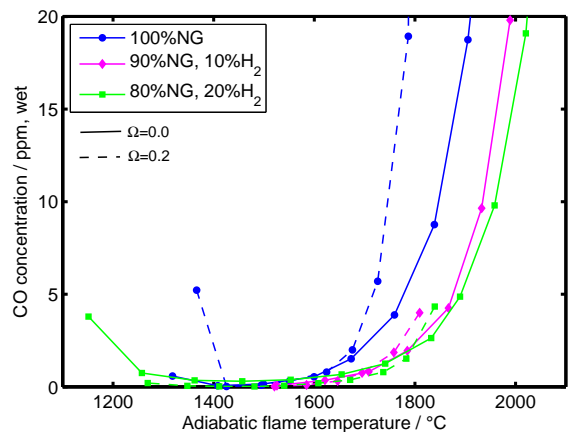


FIGURE 11: CO EMISSIONS FOR DIFFERENT FUELS

Equation 7 is an exothermal reaction; the equilibrium is moved to the left hand side of the equation for a higher gas temperature. Thus, the CO concentration increases with the flame

temperature. This also explains the increased CO emissions at wet conditions, which is caused by the higher exhaust gas temperature, due to the increased heat capacity of the gas (for the same adiabatic flame temperature, the exhaust gas temperature at humid conditions is higher than at dry conditions). A conclusion about the influence of the steam on CO emissions by changes in the OH radical concentration cannot be drawn from the measurement results.

CO emissions are reduced with increasing hydrogen concentration in the fuel, which is due to the lower concentration of CO₂ in the exhaust gas for these fuels, moving the chemical equilibrium to the right hand side of Equation 7.

REACTOR NETWORK MODEL

Design of Reactor Network

Based on the knowledge of the non-reacting flow field and the results from the gas-fired tests, a reactor network was designed to study the influence of steam on the combustion process. The layout of the network is shown in Fig. 1, representing the main regions of the combustor flow field (Fig. 2): the main flame zone comprising the inlet jet or flame, the ERZ, the IRZ, and the flow between both recirculation zones. The main flame zone is followed by the post-flame zone. Additional reactors to simulate the effect of incomplete fuel-air mixing were not added, since the mixing quality of the generic burner is very high.

The reactor volumes of the main flame zone were estimated from OH* chemiluminescence images of a typical flame (natural gas, $\Omega = 0$). The recirculation rates for the IRZ and the ERZ were estimated from the non-reacting flow field. This approach results in residence times of 1.5 – 2 ms for the flame and 20 – 25 ms for the recirculation zones. Scaling these values to the non-reacting conditions of the water tunnel tests (the ratio of the volumetric flow rates of water to air + steam at $\Omega = 20\%$ and 1800°C is approximately 150) yields residence times for the recirculation zones of 3 – 3.8 s. Considering the difference between residence time and decay rate (PSR assumption) and the reduced volume of the IRZ at reacting conditions (smaller value for V in the calculation of τ), these residence times seem to be in the range to be expected from the investigation of the non-reacting flow field. The volume of the post-flame zone was calculated from the experimental set-up, extending from the main flame zone to the location of the gas sampling probe.

Heat loss due to gas radiation was included for the reactors of the main flame zone, using an optical thin model for the flame reactor [37] and the model by Leckner [38] for the remaining reactors, estimating the optical mean path lengths from the reactor volumes. Convective heat transfer was included for the ERZ reactor and the 4 reactors surrounding the IRZ, which was assumed to be proportional to the gas temperature. The coefficient was chosen to match temperature measurements and remained the same for all simulations. Heat transfer in the post flame zone

was based on temperature measurements of the cooling water of the exhaust tube for each measurement point.

The same set of parameters was used for all simulations; the influence of fuel composition or humidity on the flame and the flow field is not represented in the model.

Results of Reactor Network

The reactor network calculations were performed with two different reaction mechanisms, GRI-Mech 3.0 [33] and the hydrocarbon mechanism v0.5 by Konnov [34]. For 100% hydrogen, the simulations with the GRI mechanism yielded results which were closer to the experimental data than with the Konnov mechanism. For the methane-containing fuels, both reaction mechanisms predicted similar results for CO emissions, and for NO_x emissions at dry conditions. NO_x emissions at humid conditions were predicted better by the Konnov mechanism for the methane-containing fuels.

At dry conditions and $T_{in} = 370^\circ\text{C}$, the predicted NO_x emissions agree very well with the experimental data for the whole range of different fuels (Fig. 12). In the case of 100% hydrogen, it seems that NO_x emissions might be over-predicted for higher equivalence ratios (the experimental data was limited due to flashback). However, considering that the chemical time scale of hydrogen is significantly lower compared to methane, the reactor network still seems to yield reasonable results for this fuel. At wet conditions, the predicted NO_x emissions agree well with

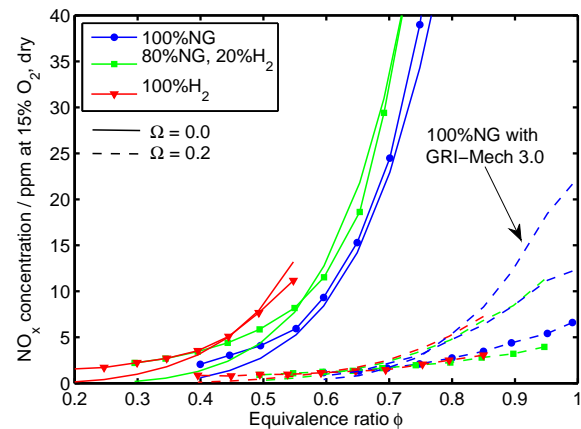


FIGURE 12: NO_x EMISSIONS: EXPERIMENT (LINES WITH MARKERS) AND SIMULATION (NO MARKERS), 100% H₂ CALCULATED WITH GRI30, THE OTHER FUELS WITH KONNOV v0.5, $T_{in} = 370^\circ\text{C}$

the experimental data for all fuels, but exhibit a stronger increase with respect to equivalence ratio. This effect is more pronounced

with the GRI mechanism. The same good agreement for all fuels and different degrees of humidity was achieved for the lower inlet temperature of 200°C with the same set of parameters for the reactor network.

A brief analysis of the NO_x formation pathways (NNH, N₂O, prompt, thermal) was performed by disabling the respective reaction equations for the 100% NG and the 100% H₂ fuels.

For the hydrogen flame at dry conditions, the formation of NO_x emissions is dominated by the NNH pathway at low temperatures, and by the thermal pathway for temperatures above 1500°C, which is also reported by Konnov et al. [39]. At wet conditions, the contribution of the NNH pathway is slightly smaller, but still dominates the overall NO_x formation. The thermal pathway is reduced even at high temperatures. Both reaction mechanisms yield similar results, with GRI-Mech predicting a slightly higher contribution of the N₂O pathway.

In the case of natural gas combustion at dry conditions, both reaction mechanisms predict the prompt pathway to be dominant up to about 1500°C, above which the thermal pathway contributes most to the total NO_x concentration. Compared to the Konnov mechanism, GRI-Mech predicts higher NO_x formation rates of the N₂O pathway at low temperatures and a higher share of the prompt pathway for higher temperatures, yet the influence on the total NO_x emissions is rather small. It has been reported in literature that the GRI mechanism over-predicts the concentration of CH, thus leading to higher prompt NO_x [36]. At wet conditions, the NNH, N₂O, and thermal pathways are significantly restrained. The prompt pathway dominates over the whole temperature range, and even more NO_x is formed through this pathway than at dry conditions (at the same flame temperature). This effect is probably caused by the increased amount of fuel in the flame to make up for the higher heat capacity of the gas to achieve the same flame temperature. The Konnov mechanism predicts the prompt NO_x to decrease with the flame temperature. The GRI mechanism, in contrast, predicts the prompt NO_x to increase with temperature, and also the contribution to the total NO_x is higher. This seems to lead to the stronger slope of NO_x emissions with respect to equivalence ratio for the simulation results with GRI-Mech 3.0 for wet conditions, leading to the over-predicted NO_x emissions (example curve for 100% NG in Fig. 12).

CO formation is controlled by reaction kinetics close to the lean blowout, where the concentration increases. For the combustor used in the current study, the range of equivalence ratios where this effect occurs is rather narrow in these experiments. The reactor network model predicts this increase in CO emissions in most cases, although it is predicted to occur at leaner conditions than in the experiment for wet conditions (Fig. 13). Towards higher equivalence ratios, the CO concentration is in the chemical equilibrium. In this region, CO formation is influenced by temperature, fuel / carbon concentration, and by OH concentration (Eq. 7). Based on the simulations, CO burnout is mostly

controlled by the exhaust gas temperature and by the equivalence ratio at the investigated operating conditions, whereas the effect of steam (changes in the OH concentration) seems to be negligible. While these calculations were performed for atmospheric conditions, increasing pressure might lead to a higher concentration of OH due to the increased third body collision efficiency of water [25].

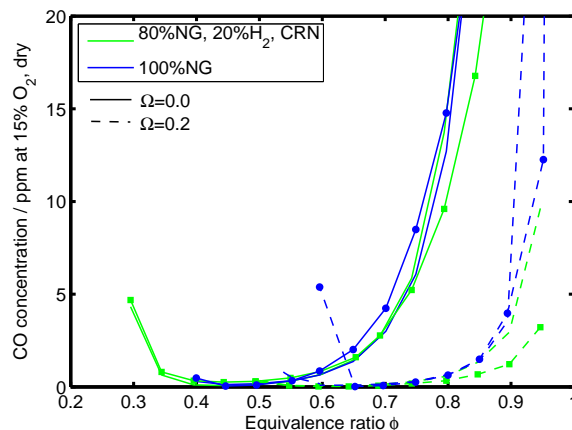


FIGURE 13: CO EMISSIONS: EXPERIMENT (LINES WITH MARKERS) AND SIMULATION (NO MARKERS), CALCULATION WITH KONNOV v0.5, $T_{in} = 370^{\circ}\text{C}$

CONCLUSIONS

The premixed combustion process of natural gas, hydrogen, and mixtures of both fuels was investigated at ultra-wet conditions. The combustor flow field, the fuel-air mixing process, and the residence times of the different regions of the combustor were investigated for non-reacting conditions. The results were also used to design a reactor network to investigate the reaction kinetics at wet conditions.

A stable flame was achieved up to a degree of humidity of 30% for natural gas and up to 50% for the hydrogen-containing fuels.

For all assessed fuels, steam was found to increase the reaction zone and move the location of flame anchoring downstream. At high steam content, the flame was widely distributed in the combustor. These effects were reduced with increasing hydrogen content of the fuel.

The risk of flashback for the hydrogen-containing fuels was lower in the presence of steam, and pure hydrogen fuel could be burnt safely up to stoichiometric conditions already at the lowest assessed degree of humidity of 10%.

NO_x emissions were significantly reduced at wet conditions. For steam contents above 20%, NO_x emissions were below 10 ppm up to stoichiometric conditions for all fuels including pure hydrogen. CO emissions were not noticeably affected by humidity.

Based on the knowledge of the non-reacting flow field and the results of the gas-fired tests, a relatively simple reactor network was developed. This model was able to predict NO_x and CO emissions over the whole range of temperatures, fuel composition, and steam content and proved to be a valuable tool in the understanding of the combustion process at ultra-wet conditions.

ACKNOWLEDGMENT

The research leading to these results has received funding from the European Research Council under the ERC grant agreement n° 247322, GREENEST.

The authors would like to thank Andy Göhrs, Phoebe Kuhn and Robert Bock for their support.

REFERENCES

- [1] Higuchi, S., Koganezawa, T., Horiuchi, Y., Araki, H., Shibata, T., and Marushima, S., 2008. "Test results from the advanced humid air turbine system pilot plant: Part I overall performance". In ASME Turbo Expo 2008, ASME Paper GT-2008-51072.
- [2] Pratt, and Whitney, 2002. Humid air turbine cycle technology development program. Technical progress report, National Energy Technology Center U.S. Department of Energy, July.
- [3] Bartlett, M., and Westermarck, M., 2005. "A study of humidified gas turbines for short-term realization in midsized power generation - Part 1: Nonintercooled cycle analysis". *Journal of Engineering for Gas Turbines and Power*, **127**, pp. 91–99.
- [4] Bartlett, M., and Westermarck, M., 2005. "A study of humidified gas turbines for short-term realization in midsized power generation - Part 2: Intercooled cycle analysis and final economic evaluation". *Journal of Engineering for Gas Turbines and Power*, **127**, pp. 100–108.
- [5] Jonsson, M., and Yan, J., 2005. "Humidified gas turbine - a review of proposed and implemented cycles". *Energy*, **30**, pp. 1013 – 1078.
- [6] Cheng, D., and Nelson, A., 2002. "The chronological development of the Cheng Cycle steam injected gas turbine during the past 25 years". In ASME Turbo Expo 2002, ASME Paper GT-2002-30119.
- [7] Bhargava, R., Bianchi, M., Campanari, S., De Pascale, A., di Montenegro, C., and Peretto, A., 2008. "High efficiency gas turbine based power cycles - a study of the most promising solutions: Part 1 - a review of the technology". In ASME Turbo Expo 2008, ASME Paper 2008-GT-51275.
- [8] Bhargava, R., Bianchi, M., Campanari, S., De Pascale, A., di Montenegro, C., and Peretto, A., 2008. "High efficiency gas turbine based power cycles - a study of the most promising solutions: Part 2 - a parametric performance evaluation". In ASME Turbo Expo 2008, ASME Paper 2008-GT-51277.
- [9] Ågren, N., Westermarck, M., Bartlett, M., and Lindquist, T., 2002. "First experiments on an evaporative gas turbine pilot power plant: Water circuit chemistry and humidification evaluation". *Journal of Engineering for Gas Turbines and Power*, **124**, pp. 96 – 102.
- [10] Araki, H., Higuchi, S., Koganezawa, T., Marushima, S., Hatamiya, S., and Tsukamoto, M., 2008. "Test results from the advanced humid air turbine system pilot plant: Part 2 humidification, water recovery and water quality". In ASME Turbo Expo 2008, ASME Paper GT-2008-51089.
- [11] Koganezawa, T., Miura, K., Saito, T., Abe, K., and Inoue, H., 2007. "Full scale testing of a cluster nozzle burner for the advanced humid air turbine". In ASME Turbo Expo 2007, ASME Paper 2007-GT-27737.
- [12] Frassoldati, A., Faravelli, T., and Ranzi, E., 2006. "A wide range modeling study of nox formation and nitrogen chemistry in hydrogen combustion". *International Journal of Hydrogen Energy*, **31**, pp. 2310–2328.
- [13] Ilbas, M., Crayford, A., Yilmaz, I., Bowen, P., and Syred, N., 2006. "Laminar-burning velocities of hydrogen-air and hydrogen-methane-air mixtures: An experimental study". *International Journal of Hydrogen Energy*, **31**, pp. 1768–1779.
- [14] Lieuwen, T., McDonell, V., Santavicca, D., and Sattelmayer, T., 2008. "Burner development and operability issues associated with steady flowing syngas fired combustors". *Combustion Science and Technology*, **180**, pp. 1169 – 1192.
- [15] Whitty, K., Zhang, H., and Eddings, E., 2008. "Emissions from syngas combustion". *Combustion Science and Technology*, **180**, pp. 1117–1136.
- [16] Richards, G. A., McMillian, M. M., Gemmen, R. S., Rogers, W. A., and Cully, S. R., 2001. "Issues for low-emission, fuel-flexible power systems". *Progress in Energy and Combustion Science*, **27**, pp. 141–169.
- [17] Dennis, R., and Harp, R., 2007. "Overview of the U.S. department of energy's office of fossil energy advanced turbine program for coal based power systems with carbon capture". In Proceedings of ASME TURBOEXPO 2007, ASME Paper 2007-GT-28338.
- [18] Lacy, B., Ziminsky, W., Lipinski, J., Varatharajan, B., Yilmaz, E., and Brumberg, J., 2008. "Low emissions combustion system development for the ge energy high hydrogen turbine program". In ASME Turbo Expo 2008, ASME Paper 2008-GT-50823.
- [19] Bancalari, E., Chan, P., and Diakunchak, I., 2007. "Advanced hydrogen gas turbine development program". In ASME Turbo Expo 2007, ASME Paper 2007-GT-27869.
- [20] Cocchi, S., Provenzale, M., Cinti, V., Carrai, L., Sigali, S., and Cappetti, D., 2008. "Experimental characterization of a hydrogen fuelled combustor with reduced nox emissions for a 10 mw class gas turbine". In ASME Turbo Expo 2008, ASME Paper 2008-GT-51271.
- [21] Mazas, A., Lacoste, D., and Schuller, T., 2010. "Experimental and numerical investigation on the laminar flame speed of ch4/o2 mixtures diluted with co2 and h2o". In ASME Turbo Expo 2010, ASME Paper 2010-GT-22512.
- [22] Dryer, F., 1976. "Water addition to practical combustion systems - concepts and applications". 16th *International Symposium on Combustion*, The Combustion Institute.
- [23] Miyauchi, T., Mori, Y., and Yamaguchi, T., 1981. "Effect of steam

- addition on NO formation". 18th *International Symposium on Combustion, The Combustion Institute*, pp. 43 – 51.
- [24] Rørtveit, G., Hustad, J., Li, S., and Williams, F., 2002. "Effects of diluents on nox formation in hydrogen counterflow flames". *Combustion and Flame*, **130**, pp. 48–61.
- [25] Zhao, D., Yamashita, H., Kitagawa, K., Arai, N., and Furuhashi, T., 2002. "Behavior and effect on NO_x formation of OH radical in methane-air diffusion flame with steam addition". *Combustion and Flame*, **130**, pp. 352–360.
- [26] Bhargava, A., Colket, M., Sowa, W., Casleton, K., and Maloney, D., 2000. "An experimental and modeling study of humid air premixed flames". *Journal of Engineering for Gas Turbines and Power*, **122**, July, pp. 405–411.
- [27] Hermann, F., Klingmann, J., and Gabrielsson, R., 2003. "Computational and experimental investigation of emissions in a highly humidified premixed flame". In ASME Turbo Expo 2003, ASME Paper GT-2003-38337.
- [28] Müller-Dethlefs, K., and Schlader, A., 1976. "The effect of steam on flame temperature, burning velocity and carbon formation in hydrocarbon flames". *Combustion and Flame*, **27**, pp. 205–215. Elsevier.
- [29] Kobayashi, H., Yata, S., Ichikawa, Y., and Ogami, Y., 2009. "Dilution effects of superheated water vapor on turbulent premixed flames at high pressure and high temperature". *Proceedings of The Combustion Institute*, **32**, pp. 2607–2614.
- [30] Gökeler, K., Göke, S., Schimek, S., and Paschereit, C., 2010. "Enhanced Recirculation in the Cold Flow Field of a Swirl-stabilized Burner for Ultra Wet Combustion". In 3rd Int. Conf. on Jets, Wakes and Separated Flows, September 27-30, Cincinnati, Ohio USA.
- [31] Lefebvre, H., 1983. *Gas Turbine Combustion*. Hemisphere Publishing Corporation.
- [32] Goodwin, D. An open source, extensible software suite for CVD process simulation. California Institute of Technology, Division of Engineering and Applied Science.
- [33] Smith, G., Golden, D., Frenklach, M., Moriarty, N., Eiteneer, B., Goldenberg, M., Bowman, C., Hanson, R., Song, S., Gardiner, W., Lissianski, V., and Q, Z. GRI-Mech 3.0. http://www.me.berkeley.edu/gri_mech/.
- [34] Konnov, A., 2000. "Development and validation of a detailed reaction mechanism for the combustion of small hydrocarbons". *Twenty-Eighth Symposium (International) on Combustion*, p. 317.
- [35] Wicksall, D., Agrawal, A., Schefer, R., and Keller, J., 2005. "The interaction of flame and flow field in a lean premixed swirl-stabilized combustor operated on h₂/ch₄/air". *Proceedings of the Combustion Institute*, **30**(2), pp. 2875–2883. ISSN 1540-7489.
- [36] Giles, D., Som, S., and Aggarwal, S., 2006. "NO_x emission characteristics of counterflow syngas diffusion flames with airstream dilution". *Fuel*, **85**, pp. 1729–1742.
- [37] Barlow, R., Karpetis, A., Frank, J., and Chen, J., 2001. "Scalar profiles and NO formation in laminar opposed-flow partially premixed methane/air flames". *Combustion and Flame*, **127**(3), pp. 2102–2118. Elsevier.
- [38] Leckner, B., 1972. "Spectral and total emissivity of water vapor and carbon dioxide". *Combustion and Flame*, **19**, pp. 33–48.
- [39] Konnov, A., Colson, G., and De Ruyck, J., 2001. "No formation rates for hydrogen combustion in stirred reactors". *Fuel*, **80**, pp. 49 – 65.